DALTON
FULL PAPER

Oxo–tungsten bis-dithiolene complexes relevant to tungsten centres in enzymes

E. Stephen Davies, Georgina M. Aston, Roy L. Beddoes, David Collison, Andrew Dinsmore, Arefa Docrat, John A. Joule, Clare R. Wilson and C. David Garner *

Chemistry Department, The University of Manchester, Oxford Road, Manchester, UK M13 9PL

Received 21st July 1998, Accepted 1st September 1998

The reaction of $[WO_2(CN)_4]^{4-}$ with a series of dimethylamino- or thione-protected asymmetric dithiolenes (ene-1,2-dithiolates) has been used to synthesise $[WO(dithiolene)_2]^{2-}$ complexes (dithiolene = $^-SC(H)C(R)S^-$, R = phenyl, pyridin-2-yl, pyridin-3-yl, pyridin-4-yl or quinoxalin-2-yl), which have been characterised by elemental analysis, spectroscopy and electrochemistry. The prototypical compound $[PPh_4]_2[WO(sdt)_2]\cdot EtOH$ [sdt = styrenedithiolate, $^-SC(H)C(Ph)S^-$], crystallises in space group $P2_1/c$ with $a = 13.242(4)$, $b = 31.894(8)$, $c = 14.589(5)$ Å, $\beta = 113.80(2)°$, and $Z = 4$. The WOS_4 moiety is square-based pyramidal with the O atom at the apex [W=O 1.724(7) Å, W–S_{av} 2.37 Å, O–W–S_{av} 108.7°] and contains a *cis* geometry of the phenyl groups, although ^{1}H NMR studies indicate that both *cis* and *trans* isomers are present in the isolated solid. The physical properties of all of the $[WO(dithiolene)_2]^{2-}$ complexes are consistent with a retention of the $W^{IV}OS_4$ centre and each system undergoes a reversible electrochemical one-electron oxidation to the corresponding W^V system. The variation in the dithiolene ^{1}H NMR resonances, ν(W=O) and ν(C=C) (dithiolene) IR stretching frequencies, and the $E_{\frac{1}{2}}$ values for the W^V–W^{IV} couple can be rationalised by a consideration of the nature of the aryl substituent. These data are compared to those of the analogous Mo^{IV} complexes and to those of the catalytic centres of the tungstoenzymes and their oxomolybdoenzyme counterparts.

Introduction

A role for tungsten in biology first emerged in the 1970s, when it was reported that tungstate stimulates the growth of certain acetate- and methane-producing microorganisms,[1] and was unequivocally demonstrated in 1983 with the purification of the first tungstoenzyme.[2] A wider role for tungsten in biology emerged in the 1990s with the recognition that this element is essential for the activity of key enzymes of hyperthermophilic archaea, organisms which thrive near 100 °C.[3] At the present time, over a dozen tungstoenzymes have been identified and purified from acetogens, methanogens, hyperthermophiles, acetylene-utilising and sulfate-reducing anaerobes.[4] Tungsten enzymes have been classified into three families: the aldehyde oxidoreductases; the formate dehydrogenases; and the acetylene hydratases. With the possible exception of the last, all of these enzymes catalyse the conversion of a substrate by net oxygen atom transfer and require the presence of tungsten.

The first protein crystallographic study of a tungstoenzyme, that of the aldehyde ferredoxin oxidoreductase (AOR) from *Pyrococcus furiosus*,[5] showed the tungsten to be coordinated by four sulfur atoms from two dithiolene groups each of which is part of a special pterin (Fig. 1). This crystallographic study was doubly significant in that it produced the first structural characterisation of this pterin which had previously been well recognised in the extensive family of the molybdoenzymes (with the notable exception of the nitrogenases) and, as such, had been labelled molybdopterin (MPT).[6] Subsequently, crystallographic studies accomplished for several oxomolybdoenzymes[7–12] have shown that the Mo is bound to one or two MPTs. A striking aspect of these crystallographic studies is the constancy of the structure of the pterin, pyran and dithiolene portions of MPT.[12]

All of the tungstoenzymes identified to date, like their molybdenum counterparts, involve the metal bound to one or two MPTs.[4] The complete nature of the coordination environment of the W has not yet been established, even for AOR of *P. furiosus*.[5] In this case, the four S-atoms from the two dithiolene groups are positioned in an approximate rectangle 'below' the tungsten but the 'apical' atom(s) was (were) not identified in the crystal structure. However, W L_{III}-edge X-ray absorption spectroscopic studies of this enzyme have indicated that the metal is coordinated to one oxo group in the 'dithionite-reduced active' form of the protein[13] and possibly two oxo groups in an oxidised inactive form.[14]

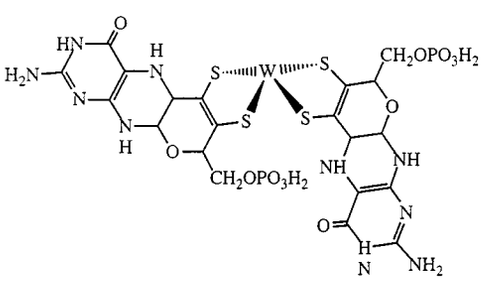

Fig. 1 Diagrammatic representation of the tungsten cofactor of aldehyde ferredoxin oxidoreductase,[5] which does not show the MPTs bridged by Mg^{2+} through the two phosphate groups. Tungsten–oxo group(s) identified by EXAFS measurements[13,14] were not located in the crystallographic determination.

Previously, we have exploited a general synthetic strategy for the synthesis of asymmetric dithiolenes[15] to prepare a series of oxobis(dithiolene)molybdenum(IV) complexes.[16] Herein we report an extension of these studies to the corresponding W systems. Comparisons of the properties of these Mo and W $[MO(dithiolene)_2]^{2-}$ complexes provide information relevant to the biochemical selection of Mo or W as the catalytic centre of particular enzymes.

Experimental

Materials

Quinoxaline, 2-, 3- and 4-acetylpyridine and phenacyl bromide were obtained from Lancaster Synthesis Ltd. The compounds $K_3Na[WO_2(CN)_4]\cdot 6H_2O$[17,18] and 2-(*N*,*N*-dimethylamino)-4-R-

1,3-dithiolium hydrogen sulfate (R = pyridin-3-yl and quinoxalin-2-yl)[19] were prepared by literature methods. 4-R-1,3-dithiol-2-one (R = phenyl, pyridin-2-yl, pyridin-3-yl, pyridin-4-yl and quinoxalin-2-yl) proligands were synthesised by application of the method of Bhattacharya and Hortmann[20] from the corresponding α-bromoketone. All reactions were performed under an atmosphere of dinitrogen or argon, using standard Schlenk line techniques. Solvents were either degassed or purged with dinitrogen or argon prior to use.

Microanalyses were accomplished by the staff of the Microanalytical Service of the Department of Chemistry, The University of Manchester. IR spectra were collected on an ATI Mattson Genesis Series FTIR spectrometer. ^{1}H NMR spectra were recorded on a Varian Unity Inova 300 or 400 instrument. Mass spectra were recorded on either a Kratos Concept 1S spectrometer (negative FAB) [matrix *m*-nitrobenzyl alcohol (*m*-NBA) or thioglycerol] or a Micromass platform (negative electrospray). EPR spectra were recorded using either a Varian E112 or Bruker ESP 300E EPR spectrometer. ENDOR spectra were recorded on a Bruker ESP 300E X-band spectrometer fitted with a Bruker ESP 360 DICE ENDOR unit. Cyclic voltammetric studies were performed on an EG&G PAR Model 362 Scanning Potentiostat with a Lloyds Instruments PL3 X-Y recorder. Pt wire working and secondary electrodes, a saturated calomel reference electrode (SCE) and the electrolyte $[NBu^n_4][BF_4]$[21] were used in the cell. Electrochemical potentials were determined relative to SCE in DMF solution at room temperature using $[CoCp_2]$ as an internal standard. Under these conditions the $E_{\frac{1}{2}}$ for the $[CoCp_2]^+$–$[CoCp_2]$ couple was measured as −852 mV and $\Delta E = 65$ mV and this was calibrated against the $E_{\frac{1}{2}}$ for the $[FeCp_2]^+$–$[FeCp_2]$ couple (495 mV and $\Delta E = 70$ mV) under the same conditions.[22] OTTLE[23] measurements were obtained using a Varian Cary 1 spectrophotometer in conjunction with a Sycopel Scientific Ltd. DD10M potentiostat. A Pt/Rh gauze working electrode, a Pt wire secondary electrode, a SCE reference electrode and the electrolyte $[NBu^n_4][BF_4]$ were used in the cell. The initial voltages were chosen to be *ca.* 100 mV more negative than the $E_{\frac{1}{2}}$ value for the respective W^V–W^{IV} couple and the final voltage *ca.* 100 mV more positive, or until the spectrum no longer changed with increasingly positive potential. The applied potential was increased in 20 mV increments from the initial voltage. The reversibility of the system was confirmed by applying the initial potential after oxidation had been completed and reproducing the initial spectrum. The OTTLE cell was calibrated against a 1 cm pathlength quartz cell using a DMF solution of $[FeCp_2]$ as the standard.[24]

Syntheses

$[PPh_4]_2[WO(sdt)_2]\cdot EtOH$ 1a. $K_3Na[WO_2(CN)_4]\cdot 6H_2O$ (0.183 g, 0.32 mmol) and NaOH (0.180 g, 4.50 mmol) were dissolved in H_2O (5 cm^3) and addition of 2-(*N*,*N*-dimethylamino)-4-phenyl-1,3-dithiolium hydrogen sulfate (0.207 g, 0.65 mmol) with EtOH (5 cm^3) was followed by reflux (2 h) generating a red solution. Filtration, then addition of $[PPh_4]Cl$ (0.241 g, 0.64 mmol) to the filtrate gave an orange-red solid. This solid was separated by decantation of the mother liquor, washed (H_2O, 2 × 15 cm^3) and dried *in vacuo*. Yield 0.136 g, 34% (Found: C, 62.38; H, 4.37; S, 10.15. Calc. for $C_{64}H_{52}OP_2S_4W\cdot C_2H_6O$: C, 63.05; H, 4.65; S, 10.18%). ^{1}H NMR {300 MHz, $(CD_3)_2SO$ containing $[CoCp_2]$} δ 8.00–7.71 (m, 44H, $[PPh_4]^+$, H-2, H-6), 7.22 (m, 4H, H-3, H-5), 7.02 (m, 4H, H-4, $H_{dithiolene}$). Mass spectrum (negative ion FAB): *m*/*z* 532 $[WO(sdt)_2]^-$.

$[PBu^n_4]_2[WO(sdt)_2]$ 1b. This was prepared by a method similar to that used for **1a** but using $[PBu^n_4]Br$. 4-Phenyl-1,3-dithiol-2-one was used as the ligand precursor and the product was isolated as a red oil. ^{1}H NMR (300 MHz, CD_3CN containing $[CoCp_2]$) δ 7.96 (d, 4H, H-2, H-6), 7.30 (m, 4H, H-3, H-5), 7.18, 7.17_5 (2 × s, 2 × 1H, $H_{dithiolene}$), 7.12 (m, 2H, H-4), 2.08 (m, 16H, $PCH_2CH_2CH_2CH_3$), 1.44 (m, 32H, $PCH_2CH_2CH_2CH_3$), 0.93 (m, 24H, $PCH_2CH_2CH_2CH_3$). Mass spectrum (negative ion FAB): *m*/*z* 532 $[WO(sdt)_2]^-$, 791 $[WO(sdt)_2 + PBu^n_4]^-$.

$[PPh_4]_2[WO(2\text{-}pedt)_2]\cdot EtOH$ 2a. $K_3Na[WO_2(CN)_4]\cdot 6H_2O$ (0.059 g, 0.10 mmol) and NaOH (0.058 g, 1.45 mmol) were dissolved in H_2O (5 cm^3). Addition of 4-(pyridin-2′-yl)-1,3-dithiol-2-one (0.042 g, 0.22 mmol) and EtOH (5 cm^3) followed by reflux (2 h) generated a dark red solution. A solution of $[PPh_4]Cl$ (0.084 g, 0.22 mmol) in H_2O (2 cm^3) was added to the hot reaction mixture. Cooling and the addition of H_2O (*ca.* 10 cm^3) gave, on prolonged stirring, a green-brown solid. The solid was separated, washed (H_2O, 3 × 10 cm^3) and dried *in vacuo*. Yield 0.045 g, 35% (Found: C, 60.41; H, 4.10; N, 2.28; S, 10.18. Calc. for $C_{62}H_{50}N_2OP_2S_4W\cdot C_2H_6O$: C, 61.04; H, 4.48; N, 2.22; S, 10.18%). ^{1}H NMR {300 MHz, $(CD_3)_2SO$ containing $[CoCp_2]$} δ 8.37 (m, 2H, H-6), 8.10 (m, 2H, H-3), 8.02–7.74 (m, 42H, $[PPh_4]^+$, $H_{dithiolene}$), 7.66 (m, 2H, H-4), 6.98 (m, 2H, H-5). Mass spectrum (negative ion FAB): *m*/*z* 534 $[WO(2\text{-}pedt)_2]^-$.

$[PBu^n_4]_2[WO(2\text{-}pedt)_2]$ 2b. This was prepared by a similar method to that of **2a** from $[PBu^n_4]Br$ and was isolated as a red oil. ^{1}H NMR {400 MHz, CD_3CN containing $[CoCp_2]$} δ 8.48 (m, 2H, H-6), 8.30 (m, 2H, H-3), 8.02, 8.01_6 (2 × s, 2 × 1H, $H_{dithiolene}$), 7.72 (m, 2H, H-4), 7.07 (m, 2H, H-5), 2.08 (m, 16H, $PCH_2CH_2CH_2CH_3$), 1.46 (m, 32H, $PCH_2CH_2CH_2CH_3$), 0.96 (m, 24H, $PCH_2CH_2CH_2CH_3$). Mass spectrum (negative ion FAB): *m*/*z* 534 $[WO(2\text{-}pedt)_2]^-$.

$[PPh_4]_2[WO(3\text{-}pedt)_2]\cdot EtOH$ 3a. This compound was prepared as for **1a** from $K_3Na[WO_2(CN)_4]\cdot 6H_2O$ (0.156 g, 0.27 mmol), NaOH (0.156 g, 3.90 mmol) and 2-(*N*,*N*-dimethylamino)-4-(pyridin-3-yl)-1,3-dithiolium hydrogen sulfate (0.175 g, 0.55 mmol). Addition of $[PPh_4]Cl$ (0.206 g, 0.55 mmol) to the red reaction mixture gave the product as a brown solid. Yield 0.149 g, 43% (Found: C, 60.6; H, 4.5; N, 2.4; S, 10.1. Calc. for $C_{62}H_{50}N_2OP_2S_4W\cdot C_2H_6O$: C, 61.04; H, 4.48; N, 2.22; S, 10.18%). ^{1}H NMR {300 MHz, $(CD_3)_2SO$ containing $[CoCp_2]$} δ 8.98 (m, 2H, H-2), 8.23 (m, 2H, H-6), 8.12 (m, 2H, H-4), 8.02–7.73 (m, 40H, $[PPh_4]^+$), 7.26 (m, 2H, H-5), 7.16, 7.15 (2 × s, 2H, $H_{dithiolene}$). Mass spectrum (negative ion FAB): *m*/*z* 534 $[WO(3\text{-}pedt)_2]^-$.

$[PBu^n_4]_2[WO(3\text{-}pedt)_2]$ 3b. This was prepared by a similar method to that of **3a** from $[PBu^n_4]Br$. 4-(Pyridin-3-yl)-1,3-dithiol-2-one was used as the ligand precursor and the product was isolated as a red oil. ^{1}H NMR {300 MHz, CD_3CN containing $[CoCp_2]$} δ 9.16 (m, 2H, H-2), 8.32 (m, 2H, H-4, H-6), 7.36, 7.35 (2 × s, 2 × 1H, $H_{dithiolene}$), 7.32 (m, 2H, H-5), 2.08 (m, 16H, $PCH_2CH_2CH_2CH_3$), 1.48 (m, 32H, $PCH_2CH_2CH_2CH_3$), 0.97 (m, 24H, $PCH_2CH_2CH_2CH_3$). Mass spectrum (negative ion FAB): *m*/*z* 533 $[WO(3\text{-}pedt)_2 - H]^-$.

$[PPh_4]_2[WO(4\text{-}pedt)_2]\cdot EtOH$ 4a. This compound was prepared as for **1a** from $K_3Na[WO_2(CN)_4]\cdot 6H_2O$ (0.151 g, 0.27 mmol), NaOH (0.182 g, 4.55 mmol) and 2-(*N*,*N*-dimethylamino)-4-(pyridin-4-yl)-1,3-dithiolium hydrogen sulfate (0.169 g, 0.53 mmol). Addition of $[PPh_4]Cl$ (0.199 g, 0.53 mmol) to the red reaction mixture gave the product as a green microcrystalline solid. Yield 0.076 g, 23% (Found: C, 60.76; H, 4.19; N, 2.29; S, 10.40. Calc. for $C_{62}H_{50}N_2OP_2S_4W\cdot C_2H_6O$: C, 61.04; H, 4.48; N, 2.22; S, 10.18%). ^{1}H NMR {300 MHz, $(CD_3)_2SO$ containing $[CoCp_2]$} δ 8.35 (m, 4H, H-2, H-6), 8.02–7.73 (m, 44H, $[PPh_4]^+$, H-3, H-5), 7.47, 7.46 (2 × s, 2H, $H_{dithiolene}$). Mass spectrum (negative ion FAB): *m*/*z* 534 $[WO(4\text{-}pedt)_2]^-$.

$[PBu^n_4]_2[WO(4\text{-}pedt)_2]$ 4b. This was prepared by a similar method to that of **4a** from $[PBu^n_4]Br$. 4-(Pyridin-4-yl)-1,3-dithiol-2-one was used as the ligand precursor and the product

Table 1 Structure analysis of compound **1a**

Formula	$C_{66}H_{58}O_2P_2S_4W$
M	1257.22
Colour	Orange
Crystal system	Monoclinic
Space group	$P2_1/c$ (no. 14)
a/Å	13.242(4)
b/Å	31.894(8)
c/Å	14.589(5)
β/°	113.80(2)
U/Å^3	5637(3)
Z	4
T/K	294
D_c/g cm^{-3}	1.481
F(000)	2552
μ(Cu-Kα)/cm^{-1}	60.93
Diffractometer	Rigaku AFC5R
Crystal dimensions/mm	0.04 × 0.07 × 0.24
λ(Cu-Kα)/Å	1.54178
θ_{max}/°	60.05
Scan type	ω/2θ
Scan width	0.89 + 0.30 tan θ
Total data	8984
Unique data	8575
'Observed' data [$I > 3\sigma(I)$], N_o	5988
Least square variable, N_v	661
R[a]	0.067
R′[a]	0.068
S[a]	2.07
Difference map features/e Å^{-3}	1.67, −1.17

[a] $R = \Sigma||F_o| - |F_c||/\Sigma|F_o|$, $R' = [(\Sigma w(|F_o| - |F_c|)^2/\Sigma wF_o^2]^{0.5}$, $S = [\Sigma w(|F_o| - |F_c|)^2/(N_o - N_v)]^{0.5}$.

was isolated as a red oil. ^{1}H NMR {300 MHz, CD_3CN containing [$CoCp_2$]} δ 8.41 (m, 4H, H-2, H-6), 7.88 (m, 4H, H-3, H-5), 7.58, 7.57 (2 × s, 2 × 1H, $H_{dithiolene}$), 2.04 (m, 16H, PCH_2CH_2-CH_2CH_3), 1.44 (m, 32H, $PCH_2CH_2CH_2CH_3$), 0.94 (m, 24H, $PCH_2CH_2CH_2CH_3$). Mass spectrum (negative ion FAB): m/z 533 [WO(4-pedt)$_2$-H]$^-$, 793 [WO(4-pedt)$_2$ + PBu_4]$^-$.

[PPh_4]$_2$[WO(qedt)$_2$] 5a. 4-(Quinoxalin-2-yl)-1,3-dithiol-2-one (0.080 g, 0.32 mmol) was added, with stirring, to a solution of $CsOH\cdot H_2O$ (0.112 g, 0.67 mmol) in anhydrous MeOH (4 cm^3). After 5 min a solution of $K_3Na[WO_2(CN)_4]\cdot 6H_2O$ (0.096 g, 0.17 mmol) in H_2O (4 cm^3) was added dropwise and the reaction mixture refluxed for 1 h. The reaction mixture was then cooled and evaporated to dryness *in vacuo* giving a dark red residue. Extraction into H_2O (15 cm^3) and the dropwise addition of a solution of [PPh_4]Cl (0.128 g, 0.34 mmol) in H_2O (2 cm^3) gave a dark red solid. The solid was separated by filtration, washed (H_2O, 3 × 10 cm^3 then Et_2O, 15 cm^3) and dried *in vacuo*. Yield 0.134 g, 60% (Found: C, 60.59; H, 3.84; N, 4.66; S, 10.56. Calc. for $C_{68}H_{52}N_4OP_2S_4W$: C, 62.09; H, 3.99; N, 4.26; S, 9.75%). ^{1}H NMR {300 MHz, $(CD_3)_2SO$ containing [$CoCp_2$]} δ 9.67, 9.64 (2 × s, 2 × H, H-3), 8.18, 8.16 (2 × s, 2 × 1H, $H_{dithiolene}$), 8.00–7.60 (m, 48H, [PPh_4]$^+$, H-5, H-6, H-7, H-8). Mass spectrum (negative ion electrospray): m/z 635 [WO(qedt)$_2$ − H]$^-$.

[PBu^n_4]$_2$[WO(qedt)$_2$] 5b. This was prepared by a similar method to that for **5a** from [PBu^n_4]Br. 4-(Quinoxalin-2-yl)-1,3-dithiol-2-one was used as the ligand precursor and the product was isolated as a dark red oil. ^{1}H NMR {300 MHz, CD_3CN containing [$CoCp_2$]} δ 9.79, 9.77 (2 × s, 2 × 1H, H-3), 8.29, 8.28 (2 × s, 2 × 1H, $H_{dithiolene}$), 8.01 (m, 4H, H-5, H-8), 7.76 (m, 2H, H-6/H-7), 7.65 (m, 2H, H-6/H-7), 2.02 (m, 16H, $PCH_2CH_2CH_2CH_3$), 1.44 (m, 32H, $PCH_2CH_2CH_2CH_3$), 0.91 (m, 24H, $PCH_2CH_2CH_2CH_3$). Mass spectrum (negative ion electrospray): m/z 636 [WO(qedt)$_2$]$^-$.

Crystallography

Orange prismatic crystals of **1a** were grown by the slow diffusion of a solution of [PPh_4]Cl in EtOH into a reaction mixture. Details of the unit cell, data collection and refinement are given in Table 1. Data were collected on a Rigaku AFC5R diffractometer with graphite-monochromated Cu-Kα radiation and a 12 kW rotating anode generator at room temperature using the ω–2θ scanning technique. The data were corrected for absorption using the DIFABS program[25] and for Lorentz and polarisation effects. The intensities of three representative reflections were measured after every 150 reflections and a linear correction factor was included to account for the observed decay. The structure was solved by direct methods.[26] Non-hydrogen atoms were refined anisotropically; hydrogen atoms were included in the structure factor calculation with all C–H = 0.95 Å, and were assigned isotropic thermal parameters which were 20% greater than the equivalent B value of the atom to which they were bonded. The function minimised during least-squares refinement was $\Sigma w(|F_o| - |F_c|)^2$ using standard neutral atom dispersion factors and anomalous dispersion corrections.[27,28] All calculations were performed using the TEXSAN[29] crystallographic package of the Molecular Structure Corporation. Least-squares planes were calculated using the PLATON program.[30] CCDC reference number 186/1147.

Results

Syntheses

Previously, we have described a strategy for the synthesis of a series of [MoO{S(H)C=C(R)S}$_2$]$^{2-}$ complexes as chemical analogues for the molybdenum centre in enzymes such as DMSO reductase which have two molybdopterins ligating the metal.[16] This strategy incorporated two important developments. Firstly, the synthesis of a range of precursors to dithiolene ligands $^-$S(R)C=C(H)S$^-$ [R = Ph, pyridin-2-yl, pyridin-3-yl, pyridin-4-yl, quinoxalin-2-yl or (dimethylaminomethyleneamino)-3-methyl-4-oxo-pteridin-6-yl] and, given the general sensitivity of the ene-1,2-dithiolate group, the protection of this functionality until delivery to the metal centre. Hence, we prepared a series of dimethylamino- or thione-protected 1,3-dithiolates which, under alkaline conditions, generated the corresponding ethene-1,2-dithiolate. Secondly, use of *trans*-[$MoO_2(CN)_4$]$^{4-}$ as the metal-containing synthon allowed the preparation of oxo-bis(dithiolene)molybdenum(IV) complexes; this result contrasts with the formation of the tris-complex [Mo(sdt)$_3$] from the equivalent reaction using [MoO_2(pentane-2,4-dionate)$_2$] as the source of the metal.[31]

Herein we have extended this synthetic strategy to tungsten, forming a series of [WO{S(H)C=C(R)S}$_2$]$^{2-}$ complexes, with *trans*-[$WO_2(CN)_4$]$^{4-}$, prepared from [$W(CN)_8$]$^{4-}$ by photolysis under alkaline conditions, being the source of W^{IV}. Ligand substitution at the tungsten centre was achieved by refluxing the ligand precursor under basic conditions in aqueous ROH (R = Me or Et) with $K_3Na[WO_2(CN)_4]$. Alkaline hydrolysis achieves the deprotection of the dithiolene and avoids protonation and subsequent loss of both oxo groups from the metal centre. In contrast to the corresponding Mo chemistry, the reaction did not proceed at room temperature.

The [WO(dithiolene)$_2$]$^{2-}$ complexes so generated (Scheme 1) were isolated by the addition of [PR_4]X (R = Ph, X = Cl or Br, or R = Bu^n, X = Br). The formal oxidation state of the metal centre in [WO(dithiolene)$_2$]$^{2-}$ is IV and was retained from that of the metal in the starting material. The products were isolated, in the case of [PPh_4]$^+$ salts, as orange–red (sdt), green–brown (2-pedt), brown (3-pedt), green (4-pedt) or dark red (qedt) solids. In the case of the [PBu^n_4]$^+$ salts, prepared for the unobstructed examination of the aromatic region in the ^{1}H NMR spectra, the products were obtained as red oils. In the case of the qedt ligand (compound **5**), the synthesis proved to be less reliable than that for other systems. Both as the solid and in solution, all of the complexes were sensitive to aerial oxid-

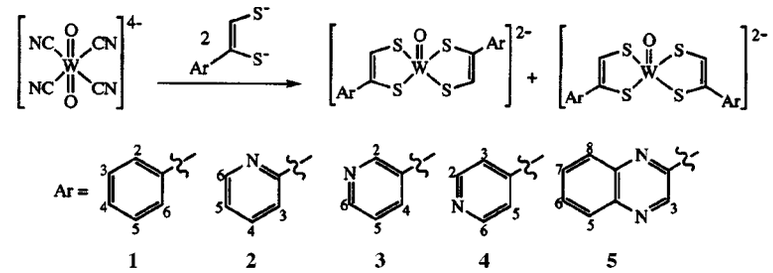

Scheme 1

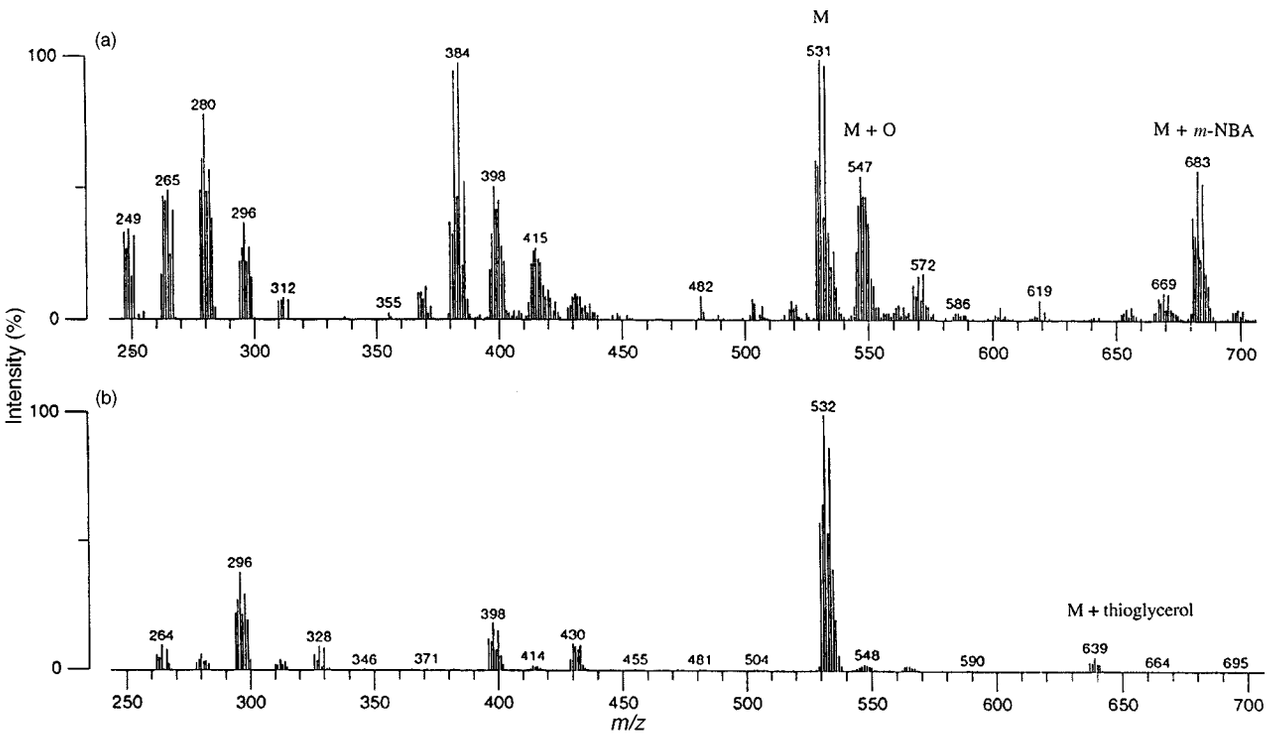

Fig. 2 FAB mass spectra of **1a** with (a) *m*-NBA and (b) thioglycerol matrix.

ation; all of the solids became red–brown and the solutions rapidly discoloured to yellow–brown.

Characterisation: analysis

The agreement between the experimental analytical data and the expected values was generally good but we note the relatively poor agreement for **5a**. However, all of the spectroscopic and electrochemical data obtained for **5a** were consistent with the formation of $[WO(qedt)_2]^{2-}$.

Mass spectrometry

Mass spectrometry (negative FAB) proved particularly valuable for the identification of these $[WO(dithiolene)_2]^{2-}$ complexes. A series of peaks with the characteristic W isotope distribution were observed at *m*/*z* values corresponding to $[WO(dithiolene)_2]^-$ in the negative ion FAB spectra. Interestingly, the choice of the matrix for sample analysis significantly affected the spectrum observed. The use of 3-nitrobenzyl alcohol (*m*-NBA) gave, in most spectra, the molecular ion (M) as well as higher *m*/*z* peaks corresponding to (M + 16) and (M + *m*-NBA), together with a significantly more complex fragmentation pattern (Fig. 2), possibly indicating a propensity for the addition of an oxo group to form a stable $\{WO_2(dithiolene)_2\}$ moiety. This effect was observed in the analogous series of Mo complexes but to a much lesser extent. The use of thioglycerol as the matrix resulted in (M) being the major W-bearing peak, although peaks associated with (M + PR_4) were observed in some of the spectra.

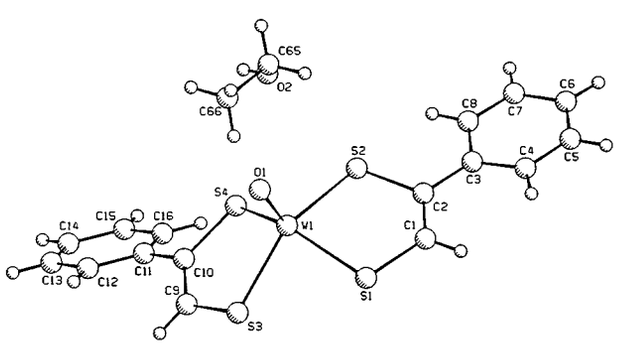

Fig. 3 Molecular structure of the dianion of **1a** showing the ethanol of crystallisation, as drawn by PLUTO.[30]

Crystallography

Compound **1a** is isomorphous with $[PPh_4]_2[MoO(sdt)_2]\cdot EtOH$;[16] the structure of the $[WO(sdt)_2]^{2-}$ anion of **1a** is illustrated in Fig. 3 and selected bond distances and angles are listed in Table 2. The WOS_4 centre has a square based pyramidal structure with the O atom at the apex; the W atom is raised above the basal plane by 0.76 Å and the mean deviation of S atoms from the basal plane is 0.05 Å. The phenyl groups of the styrenedithiolate ligands are located on the same side of the square base and this arrangement is defined as the *cis* isomer. The *trans* isomer was not observed in the single crystal X-ray diffraction analysis of **1a** but was apparent in the ^1H NMR spectra of the solutions of all of the compounds (see below).

Table 2 Selected bond distances (Å) and angles (°) for $[PPh_4]_2[WO(sdt)_2]\cdot EtOH$

W(1)–O(1)	1.724(7)	C(1)–C(2)	1.32(2)
W(1)–S(1)	2.368(3)	C(9)–C(10)	1.32(1)
W(1)–S(2)	2.362(3)	S(1)–C(1)	1.76(1)
W(1)–S(3)	2.383(3)	S(2)–C(2)	1.79(1)
W(1)–S(4)	2.367(3)	S(3)–C(9)	1.76(1)
		S(4)–C(10)	1.79(1)
O(1)–W(1)–S(1)	109.6(3)	W(1)–S(1)–C(1)	107.6(4)
O(1)–W(1)–S(2)	107.4(3)	W(1)–S(2)–C(2)	108.1(4)
O(1)–W(1)–S(3)	107.2(3)	W(1)–S(3)–C(9)	106.8(4)
O(1)–W(1)–S(4)	110.5(3)	W(1)–S(4)–C(10)	108.2(4)
S(1)–W(1)–S(2)	82.6(1)	S(1)–C(1)–C(2)	122.1(9)
S(2)–W(1)–S(4)	84.3(1)	S(2)–C(2)–C(1)	118.8(9)
S(3)–W(1)–S(4)	82.4(1)	S(3)–C(9)–C(10)	122.8(8)
S(1)–W(1)–S(3)	87.2(1)	S(4)–C(10)–C(9)	118.3(8)
C(1)–C(2)–C(3)–C(4)	−15(2)		
C(1)–C(2)–C(3)–C(8)	166(1)		
C(9)–C(10)–C(11)–C(12)	46(2)		
C(9)–C(10)–C(11)–C(16)	−134(1)		

The W=O bond distance of 1.724(7) Å is not significantly different from the values in other similar W^{IV} complexes containing the WOS_4 motif, *e.g.* $[WO(bdt)_2]^{2-}$ (bdt = benzene-1,2-dithiolate), 1.727(9) Å;[33] $[WO(mnt)_2]^{2-}$ (mnt = 1,2-dicyanoethylenedithiolate), 1.73(2) Å.[34] The mean W–S bond length of 2.37 Å is essentially the same as those in the related anions: $[WO(mnt)_2]^{2-}$ (av. 2.38 Å) and $[WO(bdt)_2]^{2-}$ (av. 2.37 Å). The average C=C (dithiolene) bond length is 1.32 Å in **1a**, the same as that in $[MoO(sdt)_2]^{2-}$.[16] The mean O–W–S interbond angle of 108.72° for **1a** is similar to that in $[WO(mnt)_2]^{2-}$ (107.8°).

The two five-membered metallocycles, defined by W(1)–S(1)–S(2)–C(1)–C(2)–C(3) and W(1)–S(3)–S(4)–C(9)–C(10)–C(11), are essentially planar (with a mean deviation from the planes of 0.08 and 0.13 Å, respectively) and subtend a dihedral angle of 47.2° within the anion which is slightly less than the corresponding angle in $[PPh_4]_2[MoO(sdt)_2]\cdot EtOH$ (49.2°). The dihedral angle between the phenyl rings, defined by C(3)–C(4)–C(5)–C(6)–C(7)–C(8) and C(11)–C(12)–C(13)–C(14)–C(15)–C(16), and the adjacent metallocycle are 18.71 and 46.93°, respectively, and this is consistent with the analogous dihedral angles in $[MoO(sdt)_2]^{2-}$ (19.37, 47.57°). The EtOH of crystallisation is outside the coordination sphere of the W but appears to be hydrogen-bonded to O(1) [O(1)···O(2) 2.82(2) Å] which compares to 2.85(1) Å for the analogous distance in $[PPh_4]_2[MoO(sdt)_2]\cdot EtOH$.[16] The dimensions of the EtOH molecule and the $[PPh_4]^+$ counter ions are unremarkable.

^{1}H NMR Spectroscopy

The air-sensitive nature of the compounds resulted in slight oxidation of the products during synthesis and/or sample preparation for spectroscopic study. Trace amounts of W^V, probably as $[WO(dithiolene)_2]^-$, resulted in a broadening of ^{1}H resonances associated with the ligands. This effect was most pronounced for the dithiolene ^{1}H resonance, as might be expected since this is the proton closest to the source of paramagnetism, the W^V centre. The observation that only a small quantity of the W^V species produced this effect suggests the presence of an efficient electron exchange process between $[WO(dithiolene)_2]^{2-}$ and $[WO(dithiolene)_2]^-$ species. The addition of small quantities of a reductant (either $Na[BH_4]$ or $[CoCp_2]$) resulted in a ^{1}H NMR spectrum of each of the $[WO(dithiolene)_2]^{2-}$ complexes with good resolution of all of the proton resonances.

The ^{1}H NMR spectra obtained for the $[PBu^n_4]^+$ salts allowed a clear view of the aromatic ^{1}H resonances of the $[WO(dithiolene)_2]^{2-}$ complexes which were observed in the following regions: δ 7.18–8.28 ($H_{dithiolene}$) and δ 7.07–9.79 ($H_{aromatic/heteroaromatic}$), the position of the former being dependent upon the nature of the Ar group (see Scheme 1). Two isomers, labelled as *cis* and *trans*, were consistently observed in these ^{1}H NMR spectra, notably with two singlets being manifest for the dithiolene protons. The chemical shift of the dithiolene protons is consistent with an aromatic electronic structure for the metallocycle and, in general, the details of the ^{1}H NMR spectra of **1**–**5** are consistent with those reported for the analogous Mo complexes.[16] For the dithiolene protons in **5**, the ^{1}H NMR spectrum showed satellite peaks (J = 10.2 Hz) due to the natural content (14.6%) of ^{183}W (Fig. 4). This value is comparable to that reported for $[W\{S(H)C{=}C(C_6H_4OMe\text{-}p)S\}_3]$ (J = 10.5 Hz).[35] Similar, less well resolved, features were observed for each of the other complexes. There is a slight solvent dependence of these ^{1}H NMR resonances and this probably derives from the solvent molecule binding *trans* to the W^{IV}=O group.

IR Spectroscopy

The IR spectra of **1**–**5** contained stretching frequencies in the regions 884–905 cm^{-1} and 1498–1519 cm^{-1} which are respectively assigned to ν(W=O) and ν(C=C) (dithiolene) stretching modes (Table 3). This range of ν(W=O) stretching frequencies is typical of complexes containing the $W^{IV}OS_4$ unit [*cf.* ν(W=O) 935 cm^{-1} in $[WO(mnt)_2]^{2-}$ [34]]. As for the corresponding Mo systems,[16] the positions of the ν(C=C) and ν(W=O) stretching frequencies are correlated; as ν(C=C) decreases ν(W=O) increases and a rationalisation of this correlation is presented below.

Electrochemistry

The cyclic voltammograms of **1**–**5** in DMF manifest two electroactive processes: a reversible, one-electron oxidation in the range −520 to −705 mV (*vs.* SCE), assigned to the $[WO(dithiolene)_2]^-$–$[WO(dithiolene)_2]^{2-}$ couple (Table 3), and an irreversible oxidation in the range 350 to 450 mV (*vs.* SCE) assigned to the $[WO(dithiolene)_2]$–$[WO(dithiolene)_2]^-$ couple. The $E_{\frac{1}{2}}$ values vary with the nature of the R group. Each W^V–W^{IV} couple is at a potential *ca.* 225 mV more negative than the corresponding Mo^V–Mo^{IV} system, a potential difference which is slightly smaller than that observed for the $[MO(bdt)_2]^-$–$[MO(bdt)_2]^{2-}$ (M = Mo, W) couples for which the $E_{\frac{1}{2}}$ values are −350 and −630 mV (*vs.* SCE), respectively.[33,36] Each irreversible $[WO(dithiolene)_2]$–$[WO(dithiolene)_2]^-$ process occurs at a potential similar to that of the corresponding Mo couple.[16]

EPR spectroscopy

EPR spectra were recorded for **1**–**5** oxidised by *ca.* one equivalent of $[FeCp_2][PF_6]$ as fluid and frozen solutions at X-band frequency and as frozen solutions at S-band frequency. The use of S-band allowed better resolution of spectra as a result of the narrower linewidths associated with the lower frequency. A comparison of the X- and S-band EPR spectra for **1** oxidised by $[FeCp_2][PF_6]$ is given in Fig. 5 which includes a simulation of the latter spectrum. The EPR spectrum of each of these W^V systems possesses essentially the same profile and the g- and A-values are the same within experimental error. In frozen solution, each EPR spectrum is rhombic (g_1 2.050, g_2 1.940, g_3 1.920); simulation assuming a coincidence of the g and A matrices yielded values for the rhombic metal hyperfine interaction of A_1 65.8×10^{-4}, A_2 36.2×10^{-4} and A_3 37.7×10^{-4} cm^{-1}. The values of the EPR parameters are very similar to those for $[WO(bdt)_2]^-$ (g_1 2.044, g_2 1.931, g_3 1.911; A_1 78×10^{-4}, A_2 40×10^{-4} and A_3 37×10^{-4} cm^{-1}).[37]

X-Band ENDOR spectra of frozen solutions (10 K) of **1**–**5**, oxidised by *ca.* one equivalent of $[FeCp_2][PF_6]$, were recorded at static field values corresponding to the turning points in the EPR spectrum. The ^{1}H ENDOR spectra of **1** are shown in Fig. 6. No signals due to the nitrogen atoms in the complex were observed. Spectra acquired with an applied magnetic field

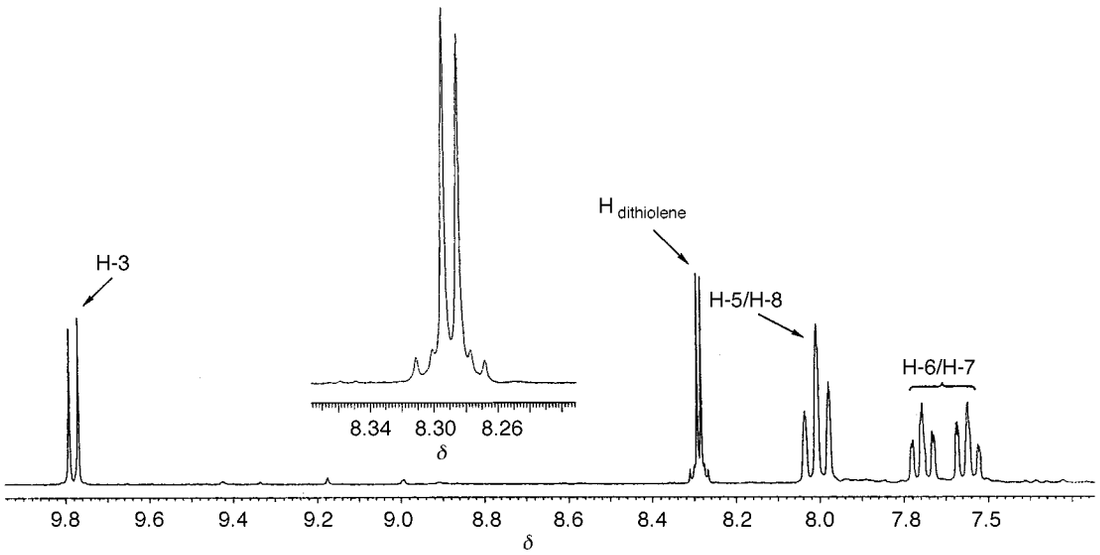

Fig. 4 The 300 MHz ^{1}H NMR spectrum of **5b** in CD_3CN in the aromatic region and an expansion of the dithiolene protons (inset).

Table 3 Selected spectroscopic and electrochemical properties of $[WO(dithiolene)_2]^{2-}$ complexes

Complex	ν(W=O)^a/cm^{-1}	ν(C=C)^a/cm^{-1}	δ($^1H_{dithiolene}$)^a	$E_{\frac{1}{2}}^c$/mV
1	884	1519	7.18^d	−705
2	905	1507	8.02	−650
3	888	1518	7.35	−615
4	905	1508	7.58	−560
5	903	1498	8.28	−520

^{a} KBr disc, as $[PPh_4]^+$ salt. ^{b} 300 MHz ^{1}H NMR spectra in CD_3CN unless stated otherwise, chemical shifts downfield from $SiMe_4$, value quoted is average position of two singlets, as $[PBu^n_4]^+$ salt. ^{c} In DMF with $[NBu^n_4][BF_4]$ as supporting electrolyte, scan rate = 100 mV s^{-1}, peak potentials *vs.* SCE, as $[PPh_4]^+$ salt. ^{d} At 400 MHz.

parallel to the g_1 or g_2 resonance positions contain an outer broad resonance with a coupling between 3.5 and 5.5 MHz. These are assigned to the dithiolene protons since their close proximity to the metal centre is consistent with a relatively large hyperfine coupling. The assignment of a similar signal observed in the ENDOR spectra of $[PPh_4][Ni(4\text{-pedt})_2]$ was confirmed by the absence of these lines after deuteration at this position.[38]

UV/VIS spectroscopy

The use of coupled spectroelectrochemical studies, in an OTTLE cell, for the collection of UV/VIS spectroscopic data has allowed the clear distinction between bands associated with $[WO(dithiolene)_2]^{2-}$ and $[WO(dithiolene)_2]^-$ complexes, some of which are weak and overlap with the bands of the other species. The information obtained is summarised in Table 4 and, as an example, the OTTLE results for **5a** are presented in Fig. 7. Table 4 also includes data for the corresponding Mo systems; these have been remeasured and the λ_{max} and ε values show some differences from the data reported previously.[16]

Discussion

The $[WO(dithiolene)_2]^{2-}$ complexes reported herein display a range of spectroscopic and redox properties which serve to characterise these species. The physical properties vary in a manner consistent with the electronic influences of the different Ar groups (see Scheme 1) operating in a $[WO(dithiolene)_2]^{n-}$ (n = 1 or 2) framework of essentially constant geometry. The aromatic character of the dithiolene protons in the $[WO(dithiolene)_2]^{2-}$ complexes is attributed to the presence of the metallocycle and is evidenced by the ^{1}H NMR resonances in the

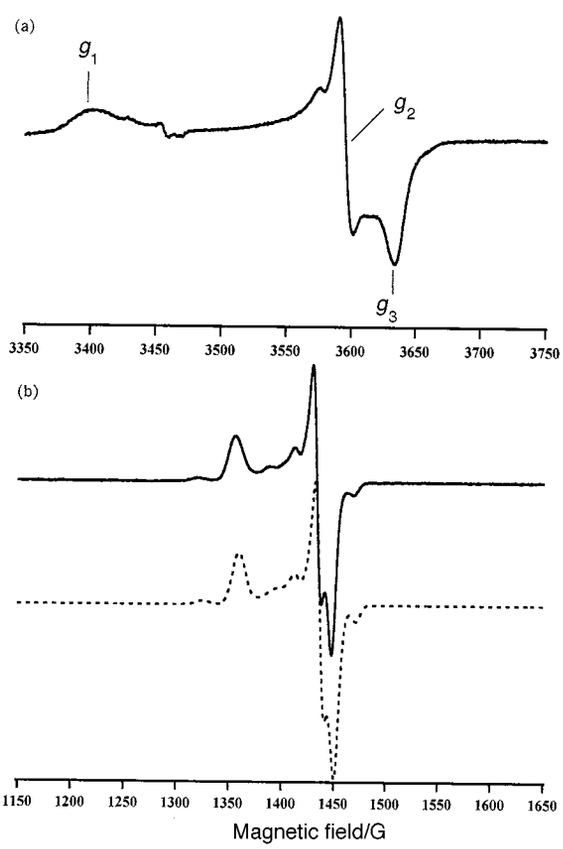

Fig. 5 (a) Experimental X-band EPR spectrum of $[WO(sdt)_2]^-$ in DMF solution at 150 K; (b) experimental S-band EPR spectrum of $[WO(sdt)_2]^-$ in DMF solution at 150 K together with simulation (dashed line) using the spin-Hamiltonian parameters $g_1 = 2.050$, $g_2 = 1.940$, $g_3 = 1.920$, $A_1 = 65.8 \times 10^{-4}$ cm^{-1}, $A_2 = 36.2 \times 10^{-4}$ cm^{-1}, $A_3 = 37.7 \times 10^{-4}$ cm^{-1} with Gaussian linewidths of $W_1 = 12$ G, $W_2 = 7$ G and $W_3 = 8$ G.

range δ 7.02–8.17 for **1a**–**5a** in $(CD_3)_2SO$ and δ 7.18–8.28 for **1b**–**5b** in CD_3CN. The relative chemical shifts of the dithiolene ^{1}H NMR resonances for complexes **1** to **5** follow the trend: **5** > **2** > **4** > **3** > **1**. This sequence corresponds to that observed for the corresponding Mo^{IV} complexes[16] with chemical shifts that are slightly (0.08–0.22 ppm) shielded with respect to their Mo analogues. As described for the Mo systems, the relative magnitude of the chemical shifts can be rationalised by a consideration of the electronic structure of these systems; specific-

Table 4 OTTLE characteristics of the $[MO(dithiolene)_2]^-$–$[MO(dithiolene)_2]^{2-}$ (M = W or Mo) couple

Compound	Potential range[a]/mV	$[MO(dithiolene)_2]^{2-}$ λ/nm (10^{-3} ε/dm^3 mol^{-1} cm^{-1})	$[MO(dithiolene)_2]^-$ λ/nm (10^{-3} ε/dm^3 mol^{-1} cm^{-1})	Isosbestic points/nm
1a	−760 to −520	464(1.9), 383(10.2), 355(14.4), 275(32.2)	706(2.2), 483(1.7), 311(14.5), 275(31.8)	584, 548, 480, 334, 310
2a	−750 to −510	384(15.7), 321(18.0), 293(27.1), 277(35.5)	688(2.4), 466(3.2), 350(13.5), 276(38.7)	447, 360, 332, 283
3a	−750 to −450	567(1.1), 485(2.0), 367(14.7), 276(33.7)	698(2.4), 315(15.3), 276(34.5)	598, 342, 306, 278
4a	−640 to −400	525(1.0), 417(6.7), 384(8.5), 292(10.9), 276(14.9)	686(1.4), 332(7.4), 276(16.7)	608, 363, 325, 284
5a	−570 to −350	497(17.2), 337(34.5), 276(46.9)	670(4.9), 412(18.6), 300(35.0), 276(49.9)	746, 587, 450, 378, 316
$[PPh_4]_2[MoO(sdt)_2]$	−560 to −300	460(3.0), 404(7.6), 362(15.5), 333(16.3), 286(29.0), 277(33.1)	844(3.4), 573(1.1), 300(21.7), 276(29.0)	469, 322, 295
$[PPh_4]_2[MoO(2\text{-}pedt)_2]$	−500 to −280	418(8.5), 390(11.8), 335(14.8), 294(23.5), 277(23.5)	830(2.1), 564(0.8), 276(22.3)	460, 352, 323, 310
$[PPh_4]_2[MoO(3\text{-}pedt)_2]$	−500 to −200	410(8.6), 374(14.2), 332(14.9), 289(21.6), 277(21.3)	833(2.7), 564(0.9), 277(20.6)	463, 328, 297
$[PPh_4]_2[MoO(4\text{-}pedt)_2]$	−460 to −200	426(8.8), 391(13.0), 341(11.6), 290(17.3), 277(18.3)	818(1.7), 573(0.7), 339(11.1), 276(17.7)	370, 310
$[PPh_4]_2[MoO(qedt)_2]$	−400 to +100	513(6.9), 338(16.6), 278(18.3)	813(1.0), 473(6.3), 400(8.4), 303(12.6), 276(18.6)	—[b]
$[PPh_4]_2[MoO(ptedt)_2]$[c]	−500 to −100	509(4.1), 387(14.5), 348(16.5), 277(12.8)	835(1.6), 446(6.8), 345(18.8), 277(11.9)	716, 480, 427, 366, 311

[a] In DMF with $[NBu^n_4][BF_4]$ as supporting electrolyte; potentials increased in 20 mV increments to the final potential; on completion of the oxidation experiment, the initial spectrum was obtained on application of the initial potential. [b] UV/VIS spectra gradually changed with increasing applied potential up to −270 mV giving isosbestic points at 394 and 496 nm. From −270 to −150 mV, new isosbestic points at 721, 461 and 381 nm were observed. [c] ptedt = $^-SC(H)C[N(Me_2NCN)CN(Me)C(O)C_2N_2C_2]S^-$.

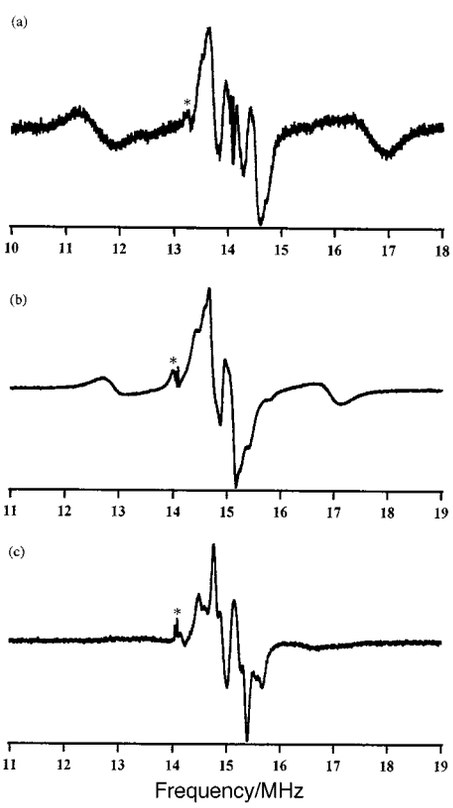

Fig. 6 ^{1}H ENDOR spectra of $[WO(sdt)_2]^-$ in deuterated DMF with a few percent deuterated toluene at 10 K, with applied magnetic field parallel to: (a) g_1 resonance position; (b) g_2 resonance position; (c) g_3 resonance position as illustrated in Fig. 5; * indicates matrix lines due to fluorine in the counter ion of the oxidant.

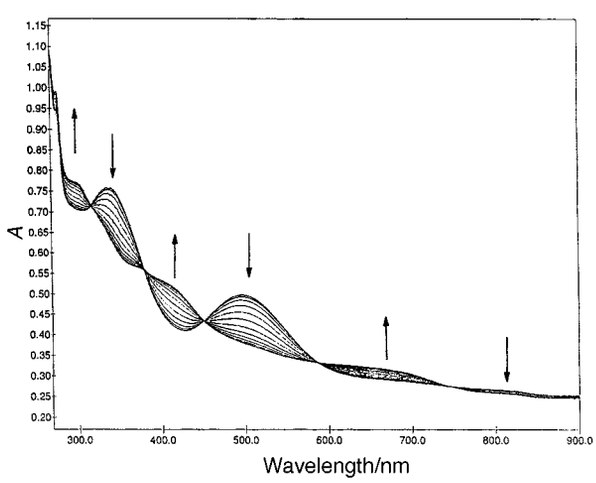

Fig. 7 UV/VIS spectra recorded using an OTTLE cell of $[WO(qedt)_2]^-$–$[WO(qedt)_2]^{2-}$ in DMF *vs.* SCE with $[NBu^n_4][BF_4]$ as supporting electrolyte and a Pt/Rh gauze working electrode. Arrows indicate the transition from W^{IV} to W^V.

ally, inductive effects and the relative ability of the R group to stabilise a resonance form in which positive charge is localised at the C atom carrying the dithiolene proton (Scheme 2, structure **A**). When R = phenyl, no such resonance forms can be written with the result that the chemical shift of the dithiolene proton in **1** is the most shielded of the series. Similarly, no such resonance form can be written when the ligand is 3-pedt, hence the dithiolene proton is the most shielded of the pyridinyl series of complexes (**2**, **3** and **4**) and the difference in dithiolene proton resonances in **1** and **3** is a measure of the relative inductive effects of the different aromatic groups. In contrast, structures **A** and **B** (Scheme 2), indicating a mesomeric drift of electron density to the nitrogen atom, can be written for **2** and **4**, respectively. Resonance forms analogous to those for **2** may be written for **5**. This results in a greater resonance effect and a resultant deshielding of the dithiolene proton chemical shift with respect to that in **3**. The downfield shift of *ca.* 0.40 ppm between the chemical shifts of the dithiolene protons of **2** and **4** can be attributed to the proximity of the nitrogen atom to the dithiolene proton. On this basis, the quinoxaline ring in **5** must exert a larger electron withdrawing effect than both the phenyl in **1** and the pyridines in **2**, **3** and **4**, for the largest deshielding effect is observed for the dithiolene ^{1}H resonance in **5**.

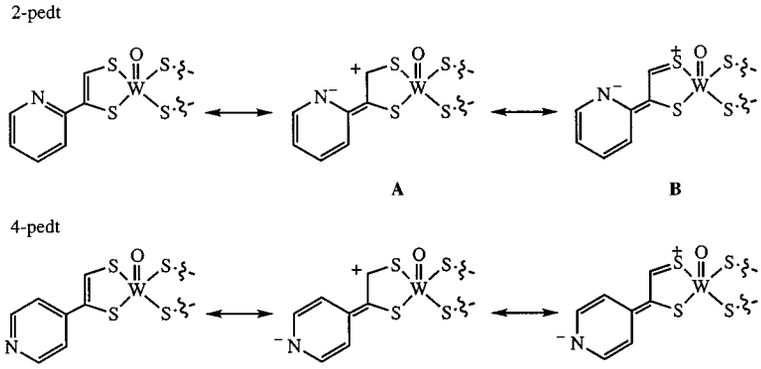

Scheme 2

ENDOR records the NMR response of a species by monitoring changes in the EPR signal. For the $[WO(dithiolene)_2]^-$ complexes, the hyperfine coupling (hfc) of the unpaired electron spin with the dithiolene proton spin, measured directly from the spectra, follows the trend **5** < **2** ≈ **4** < **3** < **1**. These relative values depend upon the electron spin density at the dithiolene proton and its distance from the metal centre. Assuming that the geometry of the systems remains the same, the greater the hfc the greater the electron density at this proton. The variation in the magnitude of the hfc is consistent with the trend observed in the chemical shifts of the dithiolene protons in the ^{1}H NMR spectra of the $[WO(dithiolene)_2]^{2-}$ complexes; an increase in the electron density at the dithiolene proton resulting in greater shielding and a decreased chemical shift. Thus, the arguments regarding inductive and mesomeric effects discussed above are consistent with the ENDOR data, strongly suggesting that similar geometries are adopted by the W^{IV} and W^{V} species. As for the corresponding Mo^{IV} systems,[16] the inductive effects and resonance forms (Scheme 2) also allow the trends observed in ν(C=C) (dithiolene) and ν(W=O) stretching frequencies to be rationalised. The ν(C=C) stretching frequency varies from 1498 cm^{-1} in **5** to 1519 cm^{-1} in **1**, as: **5** < **2** ≈ **4** < **3** ≈ **1** (Table 3) and the reverse sequence applies to the ν(W=O) values, which range from 903 cm^{-1} in **5** to 884 cm^{-1} in **1**. As the electronic structure (Scheme 2) involves a greater contribution from the resonance form with a positive charge on an S atom (structure **B**), the ν(C=C) stretching frequency is lowered due to the greater contribution from an (S)C–C(S) bond. Also, a positive charge on the S atom leads to less Sp_π–Wd_π (d_{xz}, d_{yz}) bonding, encouraging more Op_π–Wd_π bonding and increasing the ν(W=O) stretching frequency.

The general trend in the $E_{\frac{1}{2}}$ values of the W^V–W^{IV} couple (Table 3) follows from the relative inductive nature of the R groups. Thus, as the ability of the R group to stabilise the resonance forms **A** or **B** in Scheme 2 increases (*i.e.* the net electron-withdrawing nature of the R group increases), the $E_{\frac{1}{2}}$ values for the W^V–W^{IV} couple would be expected to be less negative (or more positive), *i.e.* the complex should be more difficult to oxidise. This expectation is realised in the overall sense that **1** and **5**, containing the least and most electron-withdrawing ligands, respectively, manifest the extreme $E_{\frac{1}{2}}$ values for the W^V–W^{IV} couple at −705 and −520 mV (*vs.* SCE), respectively. The variation in $E_{\frac{1}{2}}$ values within the pedt series follows the proximity of the pyridinyl nitrogen atom to the metal centre as **2** > **3** > **4**. Thus, as for the corresponding Mo systems, the overall trend in the $E_{\frac{1}{2}}$ values for the W^{VI}–W^V couple is **1** > **2** > **3** > **4** > **5**. The W^{VI}–W^V couples occur in the range which is similar to that observed for the corresponding Mo systems.[16] The irreversibility of the putative M^{VI}–M^V (M = Mo, W) couples is not unexpected since no $[MO(dithiolene)_2]$ complexes have been isolated; oxidation of MO^{2+} centres to M^{VI} invariably involves oxo-addition to produce a MO_2^{2+} centre.[33]

The low, negative potential of the reversible, one-electron W^V–W^{IV} couple required the use of the OTTLE technique to generate each oxidation state discretely in solution for the UV/VIS spectroscopic studies; this was also the situation for the Mo complexes.[16] The observation of isosbestic points in each OTTLE spectrum indicates that the oxidation of W^{IV} to W^V in these complexes occurs directly and without significant structural change, a result that might be anticipated from the known geometries of $[WO(bdt)_2]^{2-/-}$.[33] The electronic structures of the $[MO(dithiolene)_2]^{2-}$ and $[MO(dithiolene)_2]^-$ centres are considered to be $(d_{xy})^2$ and $(d_{xy})^1$, respectively.[39] The differences manifest in the UV/VIS spectra of corresponding Mo^{IV} *vs.* W^{IV} and Mo^V *vs.* W^V complexes are attributed to the different ligand field and charge transfer energies which exist for the 4d and 5d orbitals; for the EPR spectra of the M^V centres, such differences are augmented by the significantly greater spin–orbit coupling for W^V compared with Mo^V.[40] The essential invariance of the EPR spectra within each of the $[MO(dithiolene)_2]^-$ (M = Mo,[16] W) series is in stark contrast with the trends observed in NMR and IR spectroscopic and electrochemical studies of these systems. This invariance of the EPR spectrum within each series is consistent with a common structural type, the square-based pyramidal geometry, being present throughout *and* the unpaired electron of the M^V centre occupying the b_2 orbital of a C_{4v} MOS_4 moiety, orthogonal to both the S σ- and π-orbitals through which the resonance and inductive effects of the R group influence properties of the metal centre. Thus, each set of EPR properties is characteristic of the corresponding $[M^VO(dithiolene)_2]^-$ (M = Mo, W) centre with a square-based pyramidal geometry.

It is of interest to consider how the properties of these $[MO(dithiolene)_2]^{-/2-}$ (M = Mo, W) complexes relate to the nature of the catalytic centres of the molybdoenzymes and their tungsten counterparts. There is reasonably good agreement between the W=O and W–S distances derived from the W L_{III}-edge EXAFS—1.75 and 1.74 Å; 2.40 and 2.41 Å for the dithionite-reduced active and inactive AOR from *P. furiosus*[13,14] (for which the oxidation state(s) of the metal were not specified)—and the corresponding values of $[WO(sdt)_2]^{2-}$: W=O 1.724(9), W–S 2.362(3)–2.383(3) Å. Also, $[MoO(sdt)_2]^{2-}$ has Mo=O and Mo–S bond lengths[16] in good agreement with the corresponding dimensions of the DMS-reduced form (Mo^{IV})[41] of the DMSO reductase from *Rhodobacter capsulatus*,[9,41] although it must be noted that, in contrast to the five-coordinate chemical system, the site in the enzyme is seven-coordinate with DMSO and Ser(147) also bound to the Mo^{IV}. However, the angular distribution of the four S atoms about these metal centres in the enzymes is significantly different from that in the $[MO(sdt)_2]^{2-}$ complexes. Thus, the interdithiolene S–W–S angles/degrees {and corresponding S···S distances/Å} of the AOR of *P. furiosus* are (71{2.7}, 81{3.1}, 114{3.9}, 144{4.5})[42] and (84{3.2}, 87{3.3}, 139{4.5}, 145{4.5}) in $[WO(sdt)_2]^{2-}$. The former set resembles those obtained for the interdithiolene S–Mo–S angles of native (85{3.4}, 90{3.5}, 109{4.0}, 151{4.9}) and DMS-reduced (84{3.3}, 90{3.4}, 118{4.0}, 152{4.8}) DMSO-reductase from *R. capsulatus*;[43]

these values differ from those of $[MoO(sdt)_2]^{2-}$ (84{3.2}, 87{3.3}, 139{4.4}, 145{4.5})[16] which closely resemble those of $[WO(sdt)_2]^{2-}$. It is important to note that each of the distributions of the four S atoms about the Mo and W obtained from these protein crystallographic studies does not correspond to a coordination polyhedron derived from an octahedral framework. Given the difference in the angular arrangements of the S atoms, it is not surprising that none of the EPR spectra observed[4] for the W^V centre of the AOR from *P. furiosus* corresponds directly to that characteristic of a $[WO(dithiolene)_2]^-$ complex.

The redox properties of Mo centres in enzymes (the corresponding data for W centres have not yet been established) are in striking contrast to those of all chemical systems so far reported, in that the potentials of the Mo^{VI}–Mo^V and Mo^V–Mo^{IV} couples are very similar.[44] This is probably a consequence of coupled e^-/H^+ transfer occurring from one or both of these couples in the enzymes, a situation which has not yet been realised chemically.

Based on the properties of the $[MO(dithiolene)_2]^{n-}$ (M = Mo, W; n = 1,2) complexes now available, it is interesting to speculate on possible reasons for the selectivity of Mo *vs*. W (or *vice versa*) as the catalytic centre of an enzyme involving the metal bound to two 'molybdopterin' ligands. Such selectivity would not appear to operate on the basis of size, given the very similar radii of corresponding Mo^{N+} and W^{N+} centres (N = 4, 5, 6)[45] and, as an example, the dimensions of the $[MO(sdt)_2]^{2-}$ (M = Mo,[16] W) complexes are very similar. The difference in the redox potentials of corresponding Mo^V–Mo^{IV} and W^V–W^{IV} couples of *ca*. 225 mV, (see ref. 16 and Table 3) is smaller than generally observed for equivalent Mo^V–Mo^{IV} and W^V–W^{IV} couples with N-, and halogen-donor ligands[46] but is similar to that reported for the $[MO(bdt)_2]^{1-/2-}$ and $[MO(SR)_4]^{1-/2-}$ (M = Mo, W) couples.[33,47] As discussed by Holm and co-workers,[46] this relatively small difference in redox potential is presumably a consequence of the covalency of the Mo–S and W–S bonds which leads to a significant delocalisation of the electronic charge and diffuses the effect of the metal. Such a difference in redox potential may lead to one metal being favoured over the other for a particular biological role, *e.g.* to deliver redox equivalents at an optimum potential for the partner protein. Holm and co-workers[46] have shown that the relative strength of M=O (M = Mo, W) bonds favours faster atom transfer for Mo *vs*. W and this may augment selectivity based on redox potentials. Furthermore, it is now clear that there are transport proteins which specifically bind[48] Mo or W and this could lead to selective delivery of a particular metal for incorporation in cofactor biosynthesis.

Conclusions

This study has documented an extension of the general synthetic method reported previously[16] for the $[MoO(dithiolene)_2]^{2-}$ complexes to their W^{IV} counterparts. The properties of the $[WO(dithiolene)_2]^{2-}$ and $[WO(dithiolene)_2]^-$ complexes reported herein are relevant to the tungsten centres in enzymes which are bound by two 'molybdopterins' and it is important to note that the arrangement of the four S atoms in these chemical systems is significantly different from that in the one tungsten protein which has been structurally characterised.[5]

Acknowledgements

We thank EPSRC for the award of post-doctoral fellowships (G. M. A., A. D.) and a studentship (A. D.), BBSRC for the award of a fellowship (E. S. D.), Drs F. E. Mabbs and E. J. L. McInnes of the EPSRC c.w. EPR service at the University of Manchester and Dr R. D. Farley of the EPSRC ENDOR Service at the University of Wales, Cardiff for provision of facilities and valuable discussions.

References

1 L. G. Ljungdahl, *Trends Biochem. Sci.*, 1976, **1**, 63.
2 I. Yamamoto, T. Saiki, S.-M. Liu and L. G. Ljungdahl, *J. Biol. Chem.*, 1983, **258**, 1826.
3 F. O. Bryant and M. W. W. Adams, *J. Biol. Chem.*, 1989, **264**, 5070.
4 M. K. Johnson, D. C. Rees and M. W. W. Adams, *Chem. Rev.*, 1996, **96**, 2817 and references therein.
5 M. K. Chan, S. Mukund, A. Kletzin, M. W. W. Adams and D. C. Rees, *Science*, 1995, **267**, 1463.
6 K. V. Rajagopalan, *ACS Symp. Ser.*, 1993, **535**, 38.
7 M. J. Romão, M. Archer, I. Moura, J. J. G. Moura, J. LeGall, R. Engh, M. Schneider, P. Hof and R. Huber, *Science*, 1995, **167**, 1170; R. Huber, R. Duarte, I. Moura, J. J. G. Moura, J. LeGall, M. Liu, R. Hille and M. J. Romão, *Proc. Natl. Acad. Sci. USA*, 1996, **93**, 8846.
8 H. Schindelin, C. Kisker, J. Hilton, K. V. Rajagopalan and D. C. Rees, *Science*, 1996, **272**, 1615; F. Schneider, J. Löwe, R. Huber, H. Schindelin, C. Kisker and J. Knäblein, *J. Mol. Biol.*, 1996, **263**, 53; A. S. McAlpine, A. G. McEwan, A. L. Shaw and S. Bailey, *J. Biol. Inorg. Chem.*, 1997, **2**, 690.
9 A. S. McAlpine, A. G. McEwan and S. Bailey, *J. Mol. Biol.*, 1998, **275**, 613.
10 J. C. Boyington, V. Gladyshev, S. V. Khangulov, T. C. Stadtman and P. D. Sun, *Science*, 1997, **275**, 1305.
11 C. Kisker, H. Schindelin, A. Pacheco, W. Wehbi, J. H. Enemark, K. V. Rajagopalan and D. C. Rees, *Cell*, 1997, **91**, 973.
12 D. C. Rees, Y. Hu, C. Kisker and H. Schindelin, *J. Chem. Soc., Dalton Trans.*, 1997, 3909; H. Schindelin, C. Kisker and D. C. Rees, *J. Biol. Inorg. Chem.*, 1997, **2**, 773.
13 G. N. George, R. C. Prince, S. Mukund and M. W. W. Adams, results quoted in ref. 4.
14 G. N. George, R. C. Prince, S. Mukund and M. W. W. Adams, *J. Am. Chem. Soc.*, 1992, **114**, 3521.
15 D. J. Rowe, C. D. Garner and J. A. Joule, *J. Chem. Soc., Perkin Trans. 1*, 1985, 1907; A. Dinsmore, J. H. Birks, C. D. Garner and J. A. Joule, *J. Chem. Soc., Perkin Trans. 1*, 1997, 801.
16 E. S. Davies, R. L. Beddoes, D. Collison, A. Dinsmore, A. Docrat, J. A. Joule, C. R. Wilson and C. D. Garner, *J. Chem. Soc., Dalton Trans.*, 1997, 3985.
17 J. Van de Poel and H. M. Neumann, *Inorg. Chem.*, 1968, **7**, 2086.
18 S. J. Lippard and B. J. Russ, *Inorg. Chem.*, 1967, **6**, 1943.
19 D. J. Rowe, C. D. Garner and J. A. Joule, *J. Chem. Soc., Perkin Trans. 1*, 1985, 1907.
20 A. K. Bhattacharya and A. G. Hortmann, *J. Org. Chem.*, 1974, **39**, 95.
21 C. J. Pickett, *J. Chem. Soc., Chem. Commun.*, 1985, 323.
22 R. R. Gagné, G. A. Konal and G. C. Lisensky, *Inorg. Chem.*, 1980, **19**, 2854.
23 R. M. Murray, W. R. Heinemann and G. W. O'Dom, *Anal. Chem.*, 1967, **39**, 1666.
24 Y. S. Sohn, D. N. Hendrickson and H. B. Gray, *J. Am. Chem. Soc.*, 1971, **93**, 3603.
25 N. Walker and D. Stuart, *Acta Crystallogr., Sect. A*, 1983, **39**, 158.
26 G. M. Sheldrick, C. Krueger and R. Goddard, Crystallographic Computing 3, Oxford University Press, 1985, p. 175.
27 D. T. Cromer and J. T. Waber, *International Tables for X-ray Crystallography*, The Kynoch Press, 1974, vol. IV, Table 2.2A.
28 D. T. Cromer and J. T. Waber, *International Tables for X-ray Crystallography*, The Kynoch Press, 1974, vol. IV, Table 2.3.1.
29 Texan-Texray Structure Analysis Package, Molecular Structure Corporation, 1985.
30 A. L. Spek, *Acta Crystallogr., Sect. A*, 1990, **46**, C34.
31 S. Boyde, C. D. Garner, J. A. Joule and D. J. Rowe, *J. Chem. Soc., Chem. Commun.*, 1987, 800.
32 S. Motherwell and W. Clegg, PLUTO Program for Plotting Molecular and Crystal Structures, Univ. of Cambridge, 1978.
33 N. Ueyama, H. Oku and A. Nakamura, *J. Am. Chem. Soc.*, 1992, **114**, 7310.
34 S. K. Das, D. Biswas, R. Maiti and S. Sarkar, *J. Am. Chem. Soc.*, 1996, **118**, 1387.
35 D. Argyropoulos, C.-A. Mitsopoulou and D. Katakis, *Inorg. Chem.*, 1996, **35**, 5549.
36 S. Boyde, S. R. Ellis, C. D. Garner and W. Clegg, *J. Chem. Soc., Chem. Commun.*, 1986, 1541.
37 H. Oku, N. Ueyama and A. Nakamura, *Chem. Lett.*, 1995, 621.
38 A. Docrat and G. M. Aston, unpublished work.
39 C. D. Garner and S. Bristow, in *Molybdenum Enzymes*, ed. T. G. Spiro, John Wiley & Sons, New York, 1985, pp. 372–373.

40 B. N. Figgis, *Introduction to Ligand Fields*, Interscience–John Wiley & Sons, New York, 1966.
41 P. E. Baugh, C. D. Garner, J. M. Charnock, D. Collison, E. S. Davies, A. S. McAlpine, S. Bailey, I. Lane, G. R. Hanson and A. G. McEwan, *J. Biol. Inorg. Chem.*, 1997, **2**, 634.
42 Values calculated from the coordinates of the structure reported in ref. 5.
43 Values provided by S. Bailey and L. J. Stewart, personal communication.
44 R. Hille, *Chem. Rev.*, 1996, **96**, 2757.
45 R. D. Shannon, *Acta Crystallogr.*, *Sect. A*, 1976, **32**, 751.
46 G. C. Tucci, J. P. Donahue and R. H. Holm, *Inorg. Chem.*, 1998, **37**, 1602.
47 S.-L. Soong, V. Chebolm, S. A. Koch, T. O'Sullivan and M. Millar, *Inorg. Chem.*, 1986, **25**, 4068.
48 D. M. Lawson, C. E. Williams, D. J. White, A. P. Choay, L. A. Michenall and R. N. Pan, *J. Chem. Soc.*, *Dalton Trans.*, 1997, 3981.

Paper 8/05688I